Wide-Range Controllable n-Doping of Molybdenum Disulfide (MoS_2) through Thermal and Optical Activation

Hyung-Youl Park,[†] Myung-Hoon Lim,[†] Jeaho Jeon,[‡] Gwangwe Yoo,[†] Dong-Ho Kang,[†] Sung Kyu Jang,[‡] Min Hwan Jeon,[‡] Youngbin Lee,[‡] Jeong Ho Cho,[‡] Geun Young Yeom,[‡] Woo-Shik Jung,[§] Jaeho Lee,[∥] Seongjun Park,[∥] Sungjoo Lee,*[,‡,⊥] and Jin-Hong Park*[,†]

[†]Samsung-SKKU Graphene Center and School of Electronics and Electrical Engineering, Sungkyunkwan University, Suwon 440-746, Korea, [‡]SKKU Advanced Institute of Nanotechnology (SAINT), Sungkyunkwan University, Suwon 440-746, Korea, [§]Department of Electrical Engineering, Stanford University, Stanford, California 94305, United States, [∥]Samsung Advanced Institute of Technology, Samsung Electronics Co., Ltd., Yongin 446-712, Korea, and [⊥]Center for Human Interface Nanotechnology (HINT), Suwon 440-746, Korea

ABSTRACT Despite growing interest in doping two-dimensional (2D) transition metal dichalcogenides (TMDs) for future layered semiconductor devices, controllability is currently limited to only heavy doping (degenerate regime). This causes 2D materials to act as metallic layers, and an ion implantation technique with precise doping controllability is not available for these materials (*e.g.*, MoS_2, $MoSe_2$, WS_2, WSe_2, graphene). Since adjustment of the electrical and optical properties of 2D materials is possible within a light (nondegenerate) doping regime, a wide-range doping capability including nondegenerate and degenerate regimes is a critical aspect of the design and fabrication of 2D TMD-based electronic and optoelectronic devices. Here, we demonstrate a wide-range controllable n-doping method on a 2D TMD material (exfoliated trilayer and bulk MoS_2) with the assistance of a phosphorus silicate glass (PSG) insulating layer, which has the broadest doping range among the results reported to date (between 3.6×10^{10} and 8.3×10^{12} cm^{-2}) and is also applicable to other 2D semiconductors. This is achieved through (1) a three-step process consisting of, first, dopant out-diffusion between 700 and 900 °C, second, thermal activation at 500 °C, and, third, optical activation above 5 μW steps and (2) weight percentage adjustment of P atoms in PSG (2 and 5 wt %). We anticipate our widely controllable n-doping method to be a starting point for the successful integration of future layered semiconductor devices.

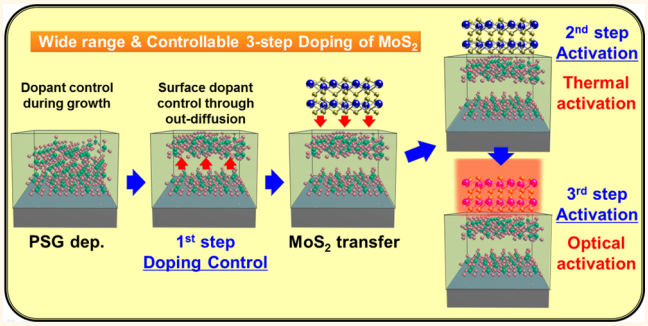

KEYWORDS: MoS_2 · wide-range · controllable doping · thermal activation · optical activation

Molybdenum disulfide (MoS_2), a transition metal dichalcogenide (TMD) with layered structure, has recently been considered a promising candidate for next-generation flexible electronic and optoelectronic devices because of its superior electrical,[1−4] optical,[5−7] and mechanical properties.[8] Thickness scalability down to a monolayer and van der Waals expitaxial structure without surface dangling bonds (consequently, native oxides) make MoS_2-based thin film transistors (TFTs) immune to the short channel effect (SCE) and provides very high field-effect mobility (~200 $cm^2/(V\ s)$, which is comparable to the universal mobility of Si), respectively.[1,9] In addition, an excellent photodetector with a wide spectral range from ultraviolet (UV) to near-infrared (IR) is achievable using MoS_2, since its energy band gap varies between 1.2 eV (bulk) and 1.8 eV (monolayer), depending on layer thickness.[6,7,9−12] It also has potential for use in chemical sensors,[13,14] memory,[15,16] and valleytronic devices.[4,5,17] However, one of the critical issues that hinder the successful integration of such MoS_2 electronic and optoelectronic devices is the lack of a reliable and controllable doping method. Such a component is essential for inducing a shift in the Fermi level, which subsequently enables wide modulations of its electrical and optical properties.[18,19]

Fang *et al.* reported a potassium-based degenerate n-doping process *via* a surface

* Address correspondence to jhpark9@skku.edu (J.-H. Park), leesj@skku.edu (S. Lee).

Received for review January 9, 2015 and accepted February 16, 2015.

Published online February 18, 2015
10.1021/acsnano.5b00153

© 2015 American Chemical Society

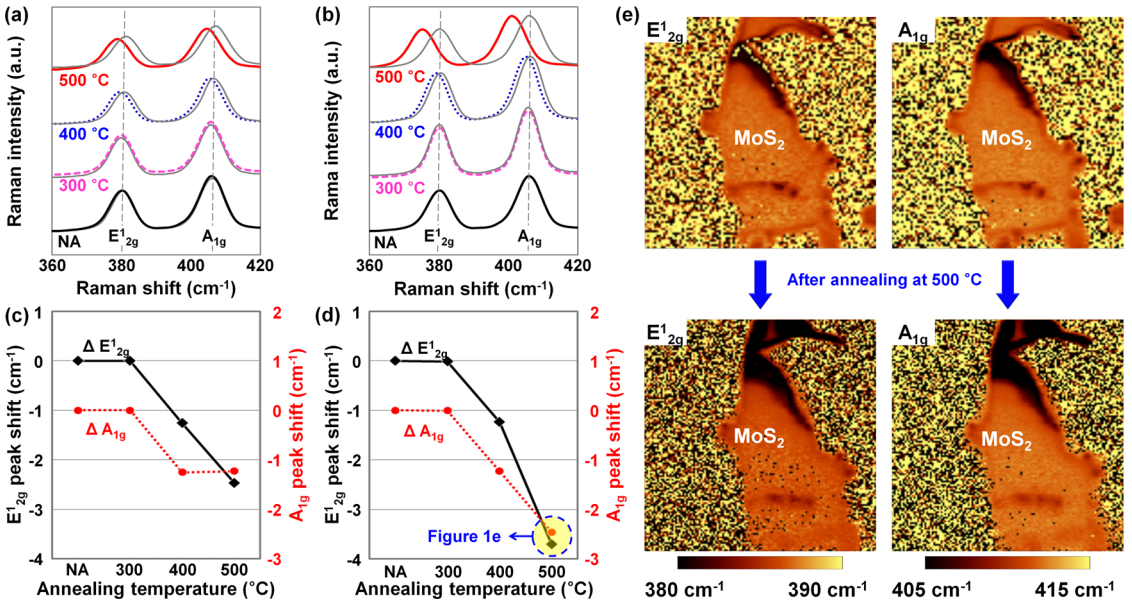

Figure 1. Raman spectrum analysis of MoS_2 on SiO_2 and PSG. Raman spectra of MoS_2 on (a) SiO_2 and (b) PSG, which were nonannealed (NA) and annealed at different temperatures (300, 400, and 500 °C). E^1_{2g} and A_{1g} peak shift data as a function of annealing temperature, which were extracted from the Raman spectra of (c) MoS_2/SiO_2 and (d) MoS_2/ PSG samples. (e) Raman mapping images in E^1_{2g} and A_{1g} peaks for the MoS_2 flake before/after the n-doping process through 500 °C annealing.

charge transfer mechanism and then used it to form highly n-doped source/drain (S/D) regions in TMD-based TFTs.[20] Sreeprasad *et al.* observed n- and p-doping phenomena on MoS_2 through different functionalization methods of Au nanoparticles.[21] In addition, n- and p-doping techniques based on polymers such as polyethylenimine (PEI) and functional self-assembled monolayers (SAMs) with different dipole moments were reported by Du *et al.*[22] and Li *et al.*[23] Chen *et al.* also presented a p-doping method on MoS_2 by using selected-area plasma treatment with fluorine (F) or oxygen (O).[24] Although Fang *et al.* controlled the doping level by adjusting the exposure time to potassium, the range of doping was limited within the heavily doped (degenerate) regime, where MoS_2 works as a near-metallic layer. Since adjusting the electrical and optical properties of MoS_2 is possible within a nondegenerate doping regime, wide-range doping capability including nondegenerate and degenerate regimes is a critical point in the design and fabrication of MoS_2-based electronic and optoelectronic devices. However, it is very challenging to achieve nondegenerate doping on 2D semiconductors and secure its wide-range doping controllability because a method such as ion implantation cannot be applied to the doping process. Recently, Lin *et al.* reported nondegenerate n-doping of MoS_2 using cesium carbonate (Cs_2CO_3).[25] In this work, we first demonstrate a wide-range controllable n-doping method for MoS_2 on a phosphorus silicate glass (PSG) insulating layer, which (1) activates the doping phenomenon *via* a thermal/optical process and (2) adjusts the doping level of MoS_2 by controlling the thermal/optical process conditions or weight percentage of P atoms during the *in situ* doped PSG growth step. This controllable n-doping process is also demonstrated on exfoliated trilayer and bulk MoS_2 films. In addition, the proposed doping method is investigated in detail through Raman spectroscopy, X-ray photoelectron spectroscopy (XPS), electrical measurements (I_D-V_G and I_D-V_D), and atomic force microscopy (AFM).

RESULTS AND DISCUSSION

Characterization of n-Doped MoS_2. First, Raman spectroscopy analysis was performed on the MoS_2/SiO_2 and MoS_2/PSG samples to investigate the effects of (1) the thermal annealing process on MoS_2 and (2) P atoms (these atoms exist in the form of phosphorus pentoxide, a chemical compound with the molecular formula P_2O_5) in the PSG layer on MoS_2, respectively, during second-step annealing. Figure 1a and b show the Raman spectra measured on MoS_2/SiO_2 and MoS_2/PSG samples with or without annealing. Here, two conventional peaks (E^1_{2g} and A_{1g}) indicating the in-plane and out-of-plane vibrations for bulk MoS_2 were respectively observed at ~380 and ~406 cm^{-1}. Then, the peak position shifts in E^1_{2g} and A_{1g} after the annealing process were extracted and plotted as a function of annealing temperature, as shown in Figure 1c and d. No shift in E^1_{2g} and A_{1g} peaks was observed for MoS_2/SiO_2 and MoS_2/PSG samples after a 300 °C annealing step compared to their initial peak positions. Although the peaks were slightly red-shifted by ~1.2 cm^{-1} for the 400 °C annealed MoS_2/PSG sample, this seems to originate from the thermal annealing effect on MoS_2 because it was also observed in the 400 °C annealed MoS_2/SiO_2 sample. This red-shift phenomenon is mainly attributed to the changes

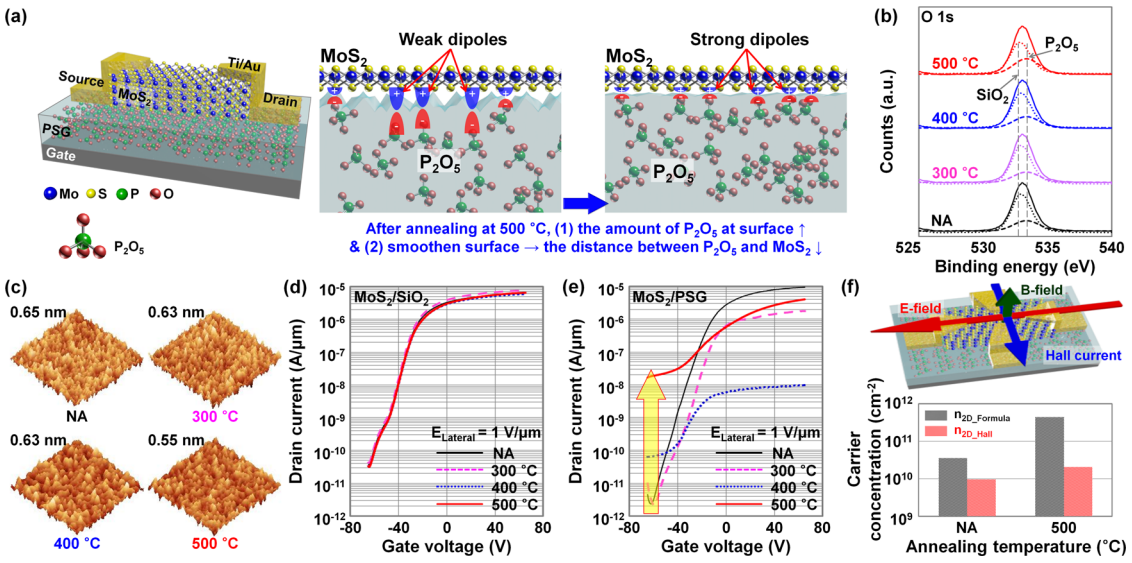

Figure 2. One-step n-doping through thermal activation. (a) Schematics of back-gated transistors fabricated on MoS_2/PSG, explaining the reaction between MoS_2 and P_2O_5 in the NA and 500 °C annealed samples. (b) XPS (O 1s peak intensity as a function of binding energy) and (c) AFM surface analysis of MoS_2 films on PSG substrates, which were nonannealed and annealed at 300, 400, and 500 °C. I_D-V_G characteristics of MoS_2 transistors fabricated on (d) SiO_2 and (e) PSG substrates, which were nonannealed and annealed at 300, 400, and 500 °C. Here, the I_D was normalized by channel width (W). (f) Comparison between the carrier concentrations obtained from the formula and the Hall-effect measurement.

in E^1_{2g} and A_{1g} mode vibrations caused by thermal expansion of MoS_2 after 400 °C annealing.[26] Similar red-shift phenomenon in the E^1_{2g} peak was previously reported by Tongay *et al.* after 450 °C annealing for 40 min, and this was possibly attributed to the desorption of contaminants or the stress-releasing effect on MoS_2.[27] However, for higher temperature annealing (500 °C), the peaks in the MoS_2/PSG sample are pushed further to the left (ΔE^1_{2g} = ~3.7 cm^{-1} and ΔA_{1g} = ~2.46 cm^{-1}) when compared with the peak shifts (ΔE^1_{2g} = ~2.47 cm^{-1} and ΔA_{1g} = ~1.23 cm^{-1}) in a MoS_2/SiO_2 sample. P_2O_5 molecules in the surface region of the PSG layer are thought to electrically affect MoS_2 after 500 °C annealing, which consequently provides more electrons to MoS_2. Sreeprasad *et al.* previously reported the red-shift of E^1_{2g} and A_{1g} peaks after the n-doping process on MoS_2, which induced functionalization of Au nanoparticles on MoS_2 through instantaneous reaction using microwave.[21] In addition, Li *et al.* observed the red-shift of the A_{1g} peak by 1.6 cm^{-1} in MoS_2 flakes on a 3-(trimethoxysilyl)-1-propanamine (APTMS)-treated substrate and confirmed the n-doping phenomenon through electrical measurements.[23] The distance between E^1_{2g} and A_{1g} peaks obtained in all of the samples in the present study was larger than 24 cm^{-1}, since measurement was done on thick MoS_2 flakes, considered bulk MoS_2. Figure 1e shows the Raman mapping images corresponding to E^1_{2g} and A_{1g} peaks before/after the n-doping process through 500 °C annealing. Darker MoS_2 images were observed after the annealing process, indicating that the MoS_2 flake was uniformly n-doped by the P atoms in PSG. Although there are color differences in each Raman mapping image, which seem to be caused by thickness variation in the exfoliated MoS_2 flake, this does not indicate nonuniformity of the n-doping concentration, because E^1_{2g} and A_{1g} peak shift values are constant at all positions despite thickness variation.

Figure 2a shows the schematics of the back-gated transistor fabricated on MoS_2 and explains the n-doping mechanism. Since the P_2O_5 molecule in the PSG layer is asymmetric in structure with nonzero dipole momentum (having a positive pole in P atoms and a negative pole in O atoms), the n-doping effect is thought to originate from another dipole induction at the MoS_2/PSG interface. The O atoms with a negative pole on the PSG surface seem to attract holes from the MoS_2 layer and hold them at the interface region, thereby n-doping the MoS_2 layer. In addition, the increased amount of P_2O_5 molecules on the PSG surface and the annealing-related surface smoothing are predicted to strengthen the dipole moment and, consequently, the degree of n-doping. As shown in Figure 2b, the XPS spectra of O 1s peaks, the intensity of the P_2O_5 signal (at 533.4 eV) increased slightly as the annealing temperature rose to 500 °C, consequently indicating the larger amount of P_2O_5 in the surface region. Figure 2c presents AFM images and surface roughness on the PSG samples, which are nonannealed or annealed between 300 and 500 °C. Although it was confirmed that P_2O_5 molecules were outdiffused from PSG film *via* annealing, the root-mean-square (RMS) roughness of the annealed PSG film was reduced from 0.65 nm to 0.55 nm as the annealing temperature increased to 500 °C due to the

high reflowing property of the PSG film. As a result, a shorter distance between P_2O_5 (particularly the negatively charged O atoms) and MoS_2 is expected in the 500 °C annealed sample when compared to other samples annealed at lower temperatures. In order to reconfirm the n-doping phenomenon on MoS_2 verified by Raman spectroscopy analysis in Figure 1, the I_D-V_G characteristics of MoS_2 transistors were measured and compared in Figures 2d and e, where the lateral electric field ($E_{Lateral}$) between the source and drain electrodes was fixed at 1 V/μm. Although shifts in E^1_{2g} and A_{1g} peaks were observed on MoS_2/SiO_2 samples that were annealed at 400 and 500 °C, no changes were observed in the I_D-V_G curves of Figure 2d, indicating that the peak shifts did not originate from the n-doping effect. However, for the case of MoS_2/PSG samples, a rising trend in off-current (2×10^{-12} A/μm → 6×10^{-11} A/μm → 2×10^{-8} A/μm at $V_{GS} = -55$ V) and a negative shift in threshold voltage (−25 V → −40 V → −42 V) were confirmed as the annealing temperature increased from 300 °C to 500 °C. Additional electrons are thought to be supplied to the MoS_2 after annealing above 400 °C because the n-doping phenomenon associated with the formation of dipoles eventually influences the tunneling of electron carriers from the source metal to MoS_2. The MoS_2 energy band is downshifted due to n-doping, which increases the electric field at the source−MoS_2 junction, thereby enhancing the tunneling of electrons and causing a negative V_{TH} shift. The increase in off-current can be explained by the interfacial charge layer caused by the dipoles, which consists of hole carriers. Although the injection of hole carriers from drain to MoS_2 is not significant even under negative V_{GS}, this conductive interfacial hole layer is expected to induce the transport of hole carriers and a subsequent increase in off-currents. This n-doping phenomenon is also present in the I_D-V_D characteristic curves (Supporting Information Figure S1) obtained for the nonannealed (NA) and the 500 °C annealed MoS_2/PSG samples. For the 500 °C annealed MoS_2/PSG device, the drain current (I_D) did not saturate as drain voltage (V_{DS}) increased, because a higher n-type carrier concentration is formed in the nonaccumulated region (between the drain electrode edge and the channel edge) after the pinch-off regime ($V_{DS} > V_{GS} - V_{TH}$). The 2D sheet doping concentration (n_{2D}) extracted from $n_{2D} = I_D L/qW\mu V_{DS}$ is also consistent with the rising trend in off-current as a function of second-step annealing temperature, showing a significant increase from 3.6×10^{10} cm^{-2} to 4.5×10^{11} cm^{-2} (Supporting Information Figure S2a). In the doping concentration equation, L and W refer to the length and width of the MoS_2 channel, respectively, q is the electron charge, μ is the field-effect mobility at $V_{GS} = 0$ V, I_D is the drain current at $V_{GS} = 0$ V, and V_{DS} is the drain−source voltage. The obtained n_{2D} values are much lower than the concentrations (1.0×10^{13} and 7.2×10^{12} cm^{-2}) achieved by the potassium[20] and APTMS[23] doping processes, which were performed on three- and one-layer MoS_2, respectively. In addition, on-currents in MoS_2/PSG devices were dramatically changed as a function of annealing temperature, unlike MoS_2/SiO_2 samples, as shown in Figure 2e. The on-current was first reduced when the annealing temperature was increased up to 400 °C, but was increased again after going through 500 °C annealing. Compared to the control and 300 °C annealed samples, more P_2O_5 molecules were expected to gather at the surface region of the PGS layer and cause a slightly stronger reaction with MoS_2. The negative poles of O atoms in P_2O_5 molecules influence the MoS_2 channel region and consequently seem to cause more severe interfacial carrier scattering, eventually decreasing on-current level and field-effect mobility in the n-channel MoS_2/PSG transistor. According to the maximum field-effect mobility extracted at $V_{DS} = 5$ V in Supporting Information Figure S2b, the initial value (10.5 cm^2 V^{-1} s^{-1}) of the control device was severely decreased down to 0.01 cm^2 V^{-1} s^{-1} when the second-step annealing temperature increased to 400 °C. However, on-current was recovered to a similar level to the control sample after 500 °C annealing, and we also confirmed that the mobility was increased up to 3.9 cm^2 V^{-1} s^{-1} in Figure S2b. It is thought that MoS_2 reacts more strongly with P_2O_5 molecules in PSG at this temperature and the large amount of electrons provided to MoS_2 consequently increase the on-current. As shown in Figure 2f, we also note that the carrier concentrations (3.6×10^{10} cm^{-2} for NA−NA and 4.5×10^{11} cm^{-2} for NA−500 °C) obtained from the formula were slightly overestimated when compared to those (9.8×10^9 cm^{-2} for NA−NA and 2.1×10^{10} cm^{-2} for NA−500 °C) obtained from Hall-effect measurement.

Two-Step n-Doping Process through Thermal Activation. To adjust the amount of P_2O_5 molecules in the surface region through out-diffusion, additional annealing steps (first annealing step) between 700 and 900 °C were performed on the PSG films in a N_2 ambient, as shown in Figure 3a. Comparing the XPS spectra for O 1s peaks between the as-deposited PSG film and the PSG films mentioned above (Figure 3b), the intensity of the P_2O_5 signal (at 533.4 eV) increased after annealing at higher temperatures. In addition, the atomic percentage of the P 2p XPS peak (at 134.58 eV) gradually increased as a function of annealing temperature (0.7% at NA, 0.77% at 700 °C, 1.74% at 800 °C, and 2.02% at 900 °C in Supporting Information Figure 3a). These indirectly indicate a higher surface concentration of P atoms and, consequently, a larger number of P_2O_5 molecules after higher temperature first-step annealing. Since it was confirmed that 500 °C annealing is the minimum requirement to activate the surface doping phenomenon, all second-step annealing after MoS_2 exfoliation was done at 500 °C. Figure 3c shows the E^1_{2g} and A_{1g} peak shifts in MoS_2 after the first and second annealing steps, which were extracted from

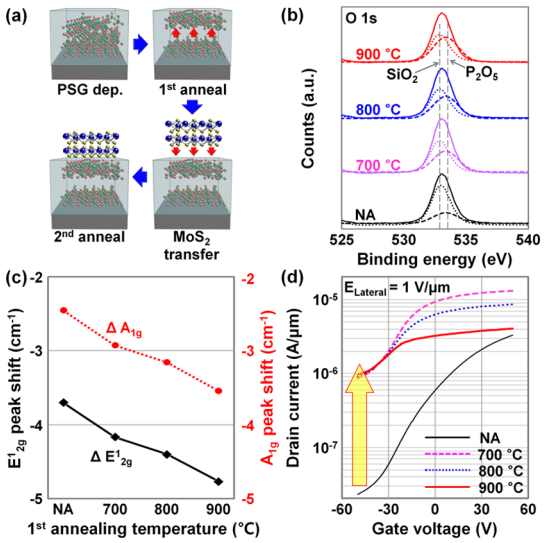

Figure 3. Two-step n-doping through thermal activation. (a) Schematic diagram showing the two-step MoS_2 doping process. (b) XPS surface analysis (O 1s peak intensity as a function of binding energy) of PSG films, which were non-annealed and annealed at 700, 800, and 900 °C (first-step annealing). (c) Extracted Raman peak shifts in E^1_{2g} and A_{1g} after the two-step MoS_2 doping process as a function of the first-step annealing temperature. (d) I_D-V_G characteristics of MoS_2 transistors fabricated without/with different first-step annealing at 700, 800, and 900 °C. Here, the I_D was normalized by channel width (W).

the MoS_2/PSG Raman spectra in Supporting Information Figure S3b. E^1_{2g} and A_{1g} peaks in the 700−500 °C (700 °C first-step and 500 °C second-step annealing) annealed MoS_2/PSG sample were more red-shifted (by ~4.17 and ~2.94 cm^{-1}) compared to the peak shifts (~3.7 and ~2.46 cm^{-1}) of the NA−500 °C (no first-step and 500 °C second-step annealing) annealed MoS_2/PSG sample. In addition, the peaks were red-shifted more and more as the first-step annealing temperature increased from 700 °C to 900 °C (~4.77 cm^{-1} in E^1_{2g} and ~3.55 cm^{-1} in A_{1g}). This indicates higher n-doping of MoS_2 due to the increase in P_2O_5 molecules in the surface region and the reduced distance between P_2O_5 and MoS_2 after first-step annealing. This doping controllability was confirmed once again by electrical measurement (I_D-V_G) of back-gated transistors fabricated on MoS_2/PSG samples. Due to the higher n-doping level achieved *via* first-step annealing, off-currents per width (at V_{GS} = −50 V and $E_{Lateral}$ = 1 V/μm) of these transistors were 8.4×10^{-7}, 8.9×10^{-7}, and 9.4×10^{-7} A/μm, which were much higher than that of the previous transistor formed on the MoS_2/PSG sample without first-step annealing (2.2×10^{-8} A/μm at V_{GS} = −50 V), indicating a higher n-doping level in the sample exposed to a higher process temperature. The extracted n_{2D} of the 900−500 °C sample was about 1.0×10^{12} cm^{-2}, which is slightly higher than that of the NA−500 °C sample (4.5×10^{11} cm^{-2}). Meanwhile, a decreasing trend in the on-current with temperature increase was observed due to the higher concentration of P atoms in the interfacial region, inducing extensive carrier scattering. On the basis of AFM analysis performed on the PSG samples (Supporting Information Figure S3c), the RMS surface roughness was reduced as the process temperature rose, owing to the high reflowing property of the PSG film. Through this, it can be predicted that interfacial scattering was mainly dominated by the Columbic scattering effect due to P atoms at the interface, not by physical scattering due to the surface roughness of the PSG. The n-doping levels that were achieved using a one- or two-step doping process were confirmed once again with XPS analysis in Supporting Information Figure S4. These upshifts observed in the 900−500 °C annealed sample (compared to NA−NA) were ~0.2 eV (Mo $3d_{5/2}$), ~0.3 eV (Mo $3d_{3/2}$), ~0.2 eV (S $2p_{1/2}$), and ~0.1 eV (S $2p_{3/2}$), directly indicating successful n-doping on MoS_2 because the Fermi level shifted toward the conduction band edge because n-doping results in a lower binding energy. Although this shift is coincident with previously reported XPS data on potassium-doped MoS_2, the degree of shift obtained by this work is smaller than that in the previous report (~0.7 eV in the Mo 3d peak and ~0.6 eV in the S 2p peak), which was degenerately doped by potassium.[20] This also indicates that the n-doping levels of our one- or two-step thermal process on PSG are in the nondegenerate regime. In addition, the achieved nondegenerate n-doping phenomenon was stable even after exposure in air for 4 days, based on the I_D-V_G characteristic of the 900−500 °C annealed device sample (Supporting Information Figure S5). As seen in the control sample (NA−NA), a small reduction in drain current also occurred in the doped device (900−500 °C).

As shown in Figure 4a, another PSG film with a lower P weight percentage (2 wt %) than the previous film (5 wt %) was used to adjust the concentration of P atoms on the surface of the PSG film and eventually the n-doping level. In this doping control experiment, first- and second-step annealing process temperatures were fixed at 900 and 500 °C, respectively, to clearly observe differences in the level of n-doping. According to XPS analysis performed on 5 and 2 wt % samples in Figure 4b and Supporting Information Figure S6a, where the intensity of P_2O_5 and P in the 2 wt % sample was lower than that in 5 wt %, a slightly lower surface concentration of P atoms (thereby, P_2O_5 molecules) in the 2 wt % sample was confirmed after first-step annealing at 900 °C. As a result, after performing second-step annealing at 500 °C to activate the n-doping phenomenon, smaller peak shifts (ΔE^1_{2g} = ~2.96 cm^{-1} and ΔA_{1g} = ~1.72 cm^{-1}) were observed in the 2 wt % sample than seen in the 5 wt % sample (ΔE^1_{2g} = ~3.7 cm^{-1} and ΔA_{1g} = ~2.46 cm^{-1}) in Figure 4c. Since the peak shifts in the 2 wt % sample were slightly larger than those (ΔE^1_{2g} = ~2.47 cm^{-1} and ΔA_{1g} = ~1.23 cm^{-1}) of the 500 °C annealed MoS_2/SiO_2 sample, MoS_2 on

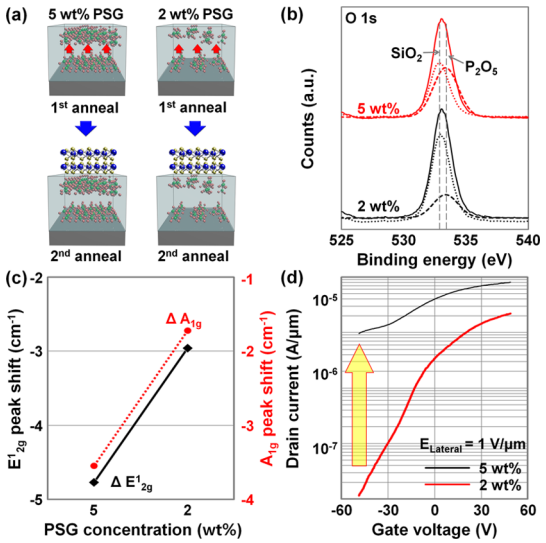

Figure 4. Two-step n-doping through thermal activation on different PSG substrates. (a) Schematic diagram showing the MoS_2 doping process performed on PSG films with different P weight percentages (5 and 2 wt %). (b) XPS surface analysis (O 1s peak intensity as a function of binding energy) of the PSG films. (c) Extracted Raman peak shifts in E^1_{2g} and A_{1g} as a function of P weight percentage. (d) I_D-V_G characteristics of MoS_2 transistors fabricated on 5 and 2 wt % PSG films. Here, the I_D was normalized by channel width (W).

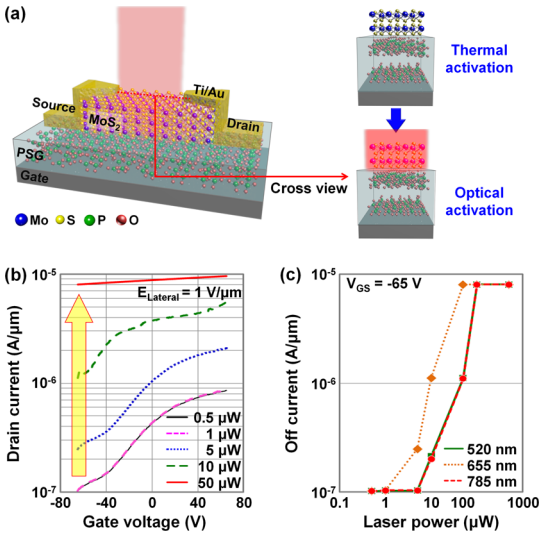

Figure 5. Three-step n-doping *via* thermal and optical activation. (a) Schematic diagrams explaining the optical MoS_2 n-doping process performed on the 900−500 °C annealed MoS_2/PSG sample. (b) I_D-V_G characteristics of MoS_2 transistors that were exposed to a 655 nm wavelength laser with power varying from 0.5 to 1000 μW. (c) Extracted off-currents (at V_{GS} = −65 V) as a function of laser power after exposing the transistors to lasers at three different wavelengths (λ = 520, 655, and 785 nm).

2 wt % PSG film is expected to be successfully n-doped at a much lower doping level. Back-gated MoS_2 transistors fabricated on the 5 and 2 wt % PSG films also demonstrate a significant difference in off-currents at $V_{GS} = -50$ V (~1.2×10^{-7} A/μm in 5 wt % and ~4.5×10^{-10} A/μm in 2 wt %) in Figure 4d, which provide evidence of the lower n-doping level of MoS_2 on 2 wt % PSG film. Although a decreasing trend was previously observed in the on-current due to the interfacial scattering effect in the high doping level regime (Figure 2), in this study, higher on-current was obtained in the 5 wt % sample with a higher surface concentration of P_2O_5. The dramatically increased number of electrons transferred from source metal to MoS_2 as the P_2O_5 concentration of PSG rose from 2 to 5 wt % has an ascendancy over the scattering effect.

Three-Step n-Doping Process *via* Thermal and Optical Activation. Additional laser exposure was performed on the 900−500 °C sample to enhance the activation of the n-doping phenomenon. Here, we also note that the second-step thermal anneal above 500 °C cannot be used to achieve higher n-doping concentration because it decomposes MoS_2 flakes even in H_2 ambient. Figure 5a shows a schematic diagram briefly explaining the optical n-doping process. When considering the energy band gap (~1.2 eV) of thick MoS_2 flakes, higher photon energy incident lasers are predicted to cause extra energy loss ($h\nu - E_g$) to reach thermal equilibrium, consequently providing heat energy to the MoS_2/PSG interface and enhancing n-doping activation. Because MoS_2 exhibits different light absorption properties as the wavelength varies, three laser sources with wavelengths of 520, 655, and 785 nm were used in this experiment. Figure 5b shows the I_D-V_G characteristics of back-gated MoS_2 transistors that were exposed to the 655 nm wavelength laser with power varying from 0.5 to 1000 μW. Although no change in the I_D-V_G curves was observed below 1 μW, the current level was increased about 70-fold when the power rose from 5 μW to 50 μW, indicating that the additional n-doping effect occurred above 5 μW for the 655 nm laser. In particular, the n-doping concentration increased from 1.0×10^{12} cm^{-2} (900−500 °C sample) to 8.3×10^{12} cm^{-2} after exposure to the 10 μW laser, and the doped MoS_2 eventually exhibited metallic properties at 50 μW. This means that the n-doping level of MoS_2 can be successfully controlled in the degenerate doping regime by adjusting the laser power. We then plotted the off-current values (at V_{GS} = −65 V) extracted from the I_D-V_G curves as a function of the laser power in Figure 5c after exposing the transistors to lasers with three different wavelengths. In the cases where 520 nm (shorter) and 785 nm (longer) wavelengths were used, the additional laser-induced n-doping phenomenon happened at a slightly higher power point of 10 μW, owing to the lower light absorption at the wavelengths than that at 655 nm. This indicates that laser wavelength adjustment, in addition to laser power adjustment, can also be a useful technique for n-doping control. For reference, we also provide I_D-V_G characteristic data for MoS_2 transistors on SiO_2 and PSG for a number of laser illumination cycles (on/off) in Supporting Information Figure S7. Although the drain current increased by laser exposure returned to the

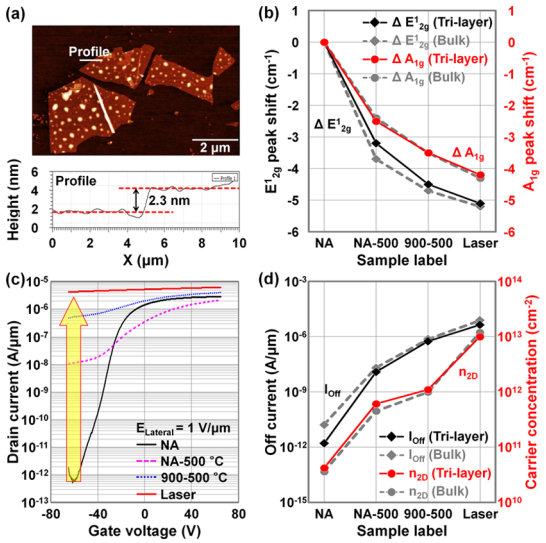

Figure 6. Three-step thermal and optical n-doping on trilayer and bulk MoS_2. (a) AFM images and height (~2.3 nm) of the trilayer MoS_2 flake. (b) Extracted Raman peak shifts in E^1_{2g} and A_{1g} obtained on trilayer and bulk MoS_2 samples (NA−NA, NA−500 °C, 900−500 °C, 900−500 °C + laser). (c) I_D−V_G characteristics of MoS_2 transistors fabricated on trilayer MoS_2 samples. Here, I_D was also normalized by channel width (W). (d) Off-currents and carrier concentrations extracted from the I_D−V_G curves of trilayer and bulk MoS_2 samples.

dark current level when the laser was turned off in devices on SiO_2, the current of the device on PSG was not altered before or after laser illumination.

Three-Step Thermal and Optical Doping on Trilayer and Bulk MoS_2. The thermal and optical doping process was performed again on trilayer MoS_2 films to determine whether a thickness effect influences n-doping. As shown in Figure 6a, the thickness of MoS_2 flakes was reduced down to ~2.3 nm (trilayer) from ~30 nm (bulk). ΔE^1_{2g} and ΔA_{1g} values extracted from Raman peaks before/after the doping process are plotted and compared with those of bulk MoS_2 in Figure 6b. The ΔE^1_{2g} and ΔA_{1g} values of trilayer MoS_2 respectively decreased to -5.1 cm^{-1} and -4.2 cm^{-1} after first-step annealing (at 900 °C) and laser treatment (λ = 655 nm and P = 1000 μW); trilayer MoS_2 showed similar behavior to bulk MoS_2 (gray dotted lines). In addition, the MoS_2 transistors fabricated under four different doping conditions (NA−NA, NA−500 °C, 900−500 °C, and 900−500 °C + laser exposure) demonstrated significantly different off-currents (~1.67×10^{-12}, ~1.25×10^{-8}, ~5.75×10^{-7}, and ~4.41×10^{-6} A/μm, respectively, at $V_{GS} = -55$ V) in Figure 6c and d. However, the increasing trend in the off-current (black solid line) is similar to that observed in the bulk MoS_2 transistors (gray dotted line). In particular, the n_{2D} values of NA−500 °C, 900−500 °C, and 900−500 °C + laser samples (trilayer MoS_2 transistors) are 6.1×10^{11}, 1.1×10^{12}, and 1.0×10^{13} cm^{-2}, which are comparable to those obtained for bulk MoS_2 transistors (4.5×10^{11}, 1.0×10^{12}, and 1.2×10^{13} cm^{-2}). These results indicate that the doping range is very broad from nondegenerate to degenerate and also the thickness of MoS_2 does not have an influence on the n-doping phenomenon. In previous cases of degenerate n-doping of MoS_2 *via* potassium[20]- and APTMS[23]-doping processes, the n-doping concentrations were 1.0×10^{13} and 7.2×10^{12} cm^{-2}, which were very similar to that of our 900−500 °C + laser sample. The doping concentration of nondegenerate n-doped MoS_2 by cesium carbonate (Cs_2CO_3) was between 1×10^{11} and 3.5×10^{11} cm^{-2},[25] which is also close to that of the NA−500 C sample.

CONCLUSIONS

In summary, a widely controllable n-doping process for MoS_2 on a PSG insulating substrate was demonstrated by adjusting the thermal and optical process conditions (T = 300−500 °C for the thermal process and P = 0.5−1000 μW for the optical process) or the concentration of P atoms in the PSG (5 and 2 wt %, thereby affecting the concentration of P_2O_5 molecules). It was confirmed that 500 °C annealing and laser exposure at 5 μW (λ = 655 nm) to 10 μW (λ = 520 and 785 nm) were the minimum requirements to activate the surface doping phenomenon. Through this, MoS_2 was uniformly n-doped by P atoms in PSG, which was confirmed through Raman spectroscopy and XPS analysis. The controlled doping levels were between 3.6×10^{10} and 8.3×10^{12} cm^{-2} before formation of a metallic layer, where MoS_2-based electronic and optoelectronic devices can be properly designed. The doping range is broadest among the results reported up to now, and also, this method is applicable to other 2D semiconductors (*e.g.*, MoS_2, $MoSe_2$, WS_2, WSe_2, graphene). This was achieved by (1) a three-step process consisting of (i) dopant out-diffusion between 700 and 900 °C, (ii) thermal activation at 500 °C, and (iii) optical activation above 5 μW steps and (2) weight percentage adjustment of P atoms (thereby, P_2O_5 molecules) in PSG. This controllable n-doping effect was also demonstrated on exfoliated trilayer and bulk MoS_2, where it was confirmed that the thickness of MoS_2 does not influence the n-doping phenomenon. We expect our wide-range controllable n-doping method to be a starting point for the successful integration of future layered semiconductor devices.

EXPERIMETAL METHODS

Preparation of PSG Films and Surface Doping Control. First, 300 nm thick PSG layers with a 5 or 2 wt % P doping concentration were deposited on a heavily doped p-type Si substrate (resistivity <0.005 Ω-m) at 480 °C in a low-pressure chemical vapor deposition (LPCVD) system. In order to control the amount of P atoms in the surface region, we performed a first-step annealing process in N_2 ambient from 700 to 900 °C.

Thermal and Optical Doping of MoS_2 on PSG Films. After transferring MoS_2 films on the annealed and nonannealed PSG samples using adhesive tape, an acetone wash was done on the samples for 1 h to remove tape residue. Then, a second-step thermal activation process was carried out in N_2/H_2 ambient from 300 to 500 °C, or optical activation (refer to Supporting Information Figure S7) was performed with laser sources at wavelengths of 520, 655, and 785 nm, in order to cause a reaction between the P atoms in the surface region of the PSG and MoS_2, eventually doping MoS_2. The doping level of MoS_2 was controlled by adjusting the second-step thermal/optical process conditions as well as regulating the weight percentage of P atoms during the *in situ* doped PSG growth step.

Characterization of Doped MoS_2 Films. The prepared MoS_2/PSG/Si samples were investigated and compared with control samples (MoS_2/SiO_2/Si) by PL/Raman spectroscopy (Alpha300 M+, WITec), XPS (ESCA200, VG Microtech Inc.), and AFM (SPA-300, Seiko Instrument) measurements. Raman spectroscopy with an excitation wavelength of 532 nm was used; its laser beam size was 0.7−0.9 μm, and the instrumental spectral resolution was below 0.9 cm^{-1}. An integration time of 5 s and spectrometry at 1800 grooves/mm were employed for the test. A Mg Kα twin-anode source and 0° of X-ray incident angle were used for XPS measurement.

Fabrication and Electrical Measurements of Undoped and Doped MoS_2 Devices. For the fabrication of back-gated MoS_2 devices (transistors and photodetectors), source/drain electrode regions were patterned on the MoS_2/PSG/Si and MoS_2/SiO_2/Si samples using optical lithography to achieve a 1 μm (or 5 μm) channel length and 1 μm (or 5 μm) channel width, followed by Ti (10 nm) and Au (50 nm) deposition *via* e-beam evaporator. For the fabrication of trilayer MoS_2 transistors, an e-beam lithography process was used instead of optical lithography. The fabricated devices were analyzed through electrical measurements (I_D-V_G and I_D-V_D) by an HP 4155B semiconductor parameter analyzer, and we subsequently calculated the carrier concentration and field-effect mobility in the MoS_2 accumulated channel using the measured data. Here, all drain currents (I_D) were normalized by channel width (W). The n_{2D} was extracted from $n_{2D} = I_D L/qW\mu V_{DS}$, where q is the electron charge, μ is the field-effect mobility at $V_{GS} = 0$ V, I_D is the drain current at $V_{GS} = 0$ V, and V_{DS} is the drain−source voltage. In addition, Hall-effect measurement was also performed to confirm the extracted n_{2D} values. For field-effect mobility extraction, the equation $\mu_{FE} = L/(WV_{DS}C_{OX}) \times (\partial I_D/\partial V_{GS})$ was used, where L and W are the length and channel width, and C_{OX} is $\varepsilon_{OX} \times \varepsilon_0/t_{OX}$, which is the gate oxide capacitance per unit area.

Conflict of Interest: The authors declare no competing financial interest.

Acknowledgment. This work was supported by the Basic Science Research Program and Midcareer Researcher Program through the National Research Foundation of Korea (NRF) funded by the Ministry of Education, Science and Technology (Grant Numbers 2011-0007997 and 2012R1A2A2A02046890).

Supporting Information Available: I_D-V_D characteristics of nonannealed and 500 °C annealed devices. Extraction of electrical parameters (carrier concentration and field-effect mobility) as a function of second-step annealing temperature (no first-step annealing). XPS, Raman spectrum, and AFM analysis of PSG films annealed at different temperatures. XPS analysis of MoS_2/PSG samples (NA, NA−500 °C, 900−500 °C). Air-stability analysis of undoped and doped MoS_2 devices. XPS and Raman spectrum analysis of PSG films with different P concentration. Experimental setup for the laser annealing process and I_D-V_G characteristics of MoS_2 transistors on SiO_2 and PSG for a number of cycles of laser illumination. This material is available free of charge *via* the Internet at http://pubs.acs.org.

REFERENCES AND NOTES

1. Radisavljevic, B.; Radenovic, A.; Brivio, J.; Giacometti, V.; Kis, A. Single-Layer MoS_2 Transistors. *Nat. Nanotechnol.* **2011**, *6*, 147–150.
2. Kim, S.; Konar, A.; Hwang, W.-S.; Lee, J. H.; Lee, J.; Yang, J.; Jung, C.; Kim, H.; Yoo, J.-B.; Choi, J.-Y.; *et al*. High-Mobility and Low-Power Thin-Film Transistors Based on Multilayer MoS_2 Crystals. *Nat. Commun.* **2012**, *3*, 1011.
3. Lembke, D.; Kis, A. Breakdown of High-Performance Monolayer MoS_2 Transistors. *ACS Nano* **2012**, *6*, 10070–10075.
4. Mak, K. F.; He, K.; Shan, J.; Heinz, T. F. Control of Valley Polarization in Monolayer MoS_2 by Optical Helicity. *Nat. Nanotechnol.* **2012**, *7*, 494–498.
5. Zeng, H.; Dai, J.; Yao, W.; Xiao, D.; Cui, X. Valley Polarization in MoS_2 Monolayers by Optical Pumping. *Nat. Nanotechnol.* **2012**, *7*, 490–493.
6. Lee, S. H.; Min, S.-W.; Chang, Y.-G.; Park, M. K.; Nam, T.; Kim, H.; Kim, J. H.; Ryu, S.; Im, S. MoS_2 Nanosheet Phototransistors with Thickness-Modulated Optical Energy Gap. *Nano Lett.* **2012**, *12*, 3695–3700.
7. Yin, Z.; Li, H.; Li, H.; Jiang, L.; Shi, Y.; Sun, Y.; Lu, G.; Zhang, Q.; Chen, X.; Zhang, H. Single-Layer MoS_2 Phototransistors. *ACS Nano* **2012**, *6*, 74–80.
8. Bertolazzi, S.; Brivio, J.; Kis, A. Stretching and Breaking of Ultrathin MoS_2. *ACS Nano* **2011**, *5*, 9703–9709.
9. Liu, W.; Kang, J.; Sarkar, D.; Khatami, Y.; Jena, D.; Banerjee, K. Role of Metal Contacts in Designing High-Performance Monolayer n-Type WSe_2 Field Effect Transistors. *Nano Lett.* **2013**, *13*, 1983–1990.
10. Mak, K. F.; Lee, C.; Hone, J.; Shan, J.; Heinz, T. F. Atomically Thin MoS_2: A New Direct-Gap Semiconductor. *Phys. Rev. Lett.* **2010**, *105*, 136805.
11. Kam, K. K.; Parkinson, B. A. Detailed Photocurrent Spectroscopy of the Semiconducting Group Vib Transition Metal Dichalcogenides. *J. Phys. Chem.* **1982**, *86*, 463–467.
12. Choi, W.; Cho, M. Y.; Konar, A.; Lee, J. H.; Cha, G.-B.; Hong, S. C.; Kim, S.; Kim, J.; Jena, D.; Joo, J.; *et al*. High-Detectivity Multilayer MoS_2 Phototransistors with Spectral Response from Ultraviolet to Infrared. *Adv. Mater.* **2012**, *24*, 5832–5836.
13. Li, H.; Yin, Z.; He, Q.; Li, H.; Huang, X.; Lu, G.; Fam, D. W. H.; Tok, A. I. Y.; Zhang, Q.; Zhang, H. Fabrication of Single- and Multilayer MoS_2 Film-Based Field-Effect Transistors for Sensing NO at Room Temperature. *Small* **2012**, *8*, 63–67.
14. Late, D. J.; Huang, Y.-K.; Liu, B.; Acharya, J.; Shirodkar, S. N.; Luo, J.; Yan, A.; Charles, D.; Waghmare, U. V.; Dravid, V. P.; *et al*. Sensing Behavior of Atomically Thin-Layered MoS_2 Transistors. *ACS Nano* **2013**, *7*, 4879–4891.
15. Bertolazzi, S.; Krasnozhon, D.; Kis, A. Nonvolatile Memory Cells Based on MoS_2/Graphene Heterostructures. *ACS Nano* **2013**, *7*, 3246–3252.
16. Choi, M. S.; Lee, G. H.; Yu, Y.-J.; Lee, D.-Y.; Lee, S. H.; Kim, P.; Hone, J.; Yoo, W. Y. Controlled Charge Trapping by Molybdenum Disulphide and Graphene in Ultrathin Heterostructured Memory Devices. *Nat. Commun.* **2013**, *4*, 1624.
17. Xiao, D.; Liu, G.-B.; Feng, W.; Xu, X.; Yao, W. Coupled Spin and Valley Physics in Monolayers of MoS_2 and Other Group-VI Dichalcogenides. *Phys. Rev. Lett.* **2012**, *108*, 196802.
18. Yu, W. J.; Li, Z.; Chen, Y.; Wang, Y.; Huang, Y.; Duan, X. Vertically Stacked Multi-Heterostructures of Layered Materials for Logic Transistors and Complementary Inverters. *Nat. Mater.* **2013**, *12*, 246–252.
19. Yu, W. J.; Liu, Y.; Zhou, H.; Yin, A.; Li, Z.; Huang, Y. Highly Efficient Gate-Tunable Photocurrent Generation in Vertical Heterostructures of Layered Materials. *Nat. Nanotechnol.* **2013**, *8*, 952–958.
20. Fang, H.; Tosun, M.; Seol, G.; Chang, T. C.; Takei, K.; Gou, J.; Javey, A. Degenerate n-Doping of Few-Layer Transition Metal Dichalcogenides by Potassium. *Nano Lett.* **2013**, *13*, 1991–1995.
21. Sreeprasad, T. S.; Nguyen, P.; Kim, N.; Berry, V. Controlled, Defect-Guided, Metal-Nanoparticle Incorporation onto MoS_2 *via* Chemical and Microwave Routes: Electrical, Thermal, and Structural Properties. *Nano Lett.* **2013**, *13*, 4434–4441.
22. Du, Y.; Liu, H.; Neal, A. T.; Si, M.; Ye, P. D. Molecular Doping of Multilayer MoS_2 Field-Effect Transistors: Reduction in

Sheet and Contact Resistances. *IEEE Electron Device Lett.* **2013**, *34*, 1328–1330.
23. Li, Y.; Xu, C.-Y.; Hu, P. A.; Zhen, L. Carrier Control of MoS_2 Nanoflakes by Functional Self-Assembled Monolayers. *ACS Nano* **2013**, *7*, 7795–7804.
24. Chen, M.; Nam, H.; Wi, S.; Ji, L.; Ren, X.; Bian, L.; Lu, S.; Liang, X. Stable Few-Layer MoS_2 Rectifying Diodes Formed by Plasma-Assisted Doping. *Appl. Phys. Lett.* **2013**, *103*, 142110.
25. Lin, J. D.; Han, C.; Wang, F.; Wang, R.; Xiang, D.; Qin, S.; Zhang, X.-A.; Wang, L.; Zhang, H.; Wee, A. T. S.; *et al.* Electron-Doping Enhanced Trion Formation in Monolayer Molybdenum Disulfide Functionalized with Cesium Carbonate. *ACS Nano* **2014**, *8*, 5323–5329.
26. Sahoo, S.; Gaur, A. P. S.; Ahmadi, M.; Guinel, M. J. F.; Katiyar, R. S. Temperature-Dependent Raman Studies and Thermal Conductivity of Few-Layer MoS_2. *J. Phys. Chem. C* **2013**, *117*, 9042–9047.
27. Tongay, S.; Zhou, J.; Ataca, C.; Liu, J.; Kang, J. S.; Matthews, T. S.; You, L.; Li, J.; Grossman, J. C.; Wu, J. Broad-Range Modulation of Light Emission in Two-Dimensional Semiconductors by Molecular Physisorption Gating. *Nano Lett.* **2013**, *13*, 2831–2836.